Title:

Chloride ions evoke taste sensations by binding to the extracellular ligand-binding domain of sweet/umami taste receptors

Authors:

Nanako Atsumi[1†], Keiko Yasumatsu[2†], Yuriko Takashina[3], Chiaki Ito[1], Norihisa Yasui[1], Robert F. Margolskee[4], Atsuko Yamashita[1]

[†]These authors contributed equally to this work.

Affiliation:

[1]Graduate School of Medicine, Dentistry and Pharmaceutical Sciences, Okayama University, Okayama, Japan, [2]Oral Health Science Center, Tokyo Dental College, Tokyo, [3]School of Pharmaceutical Sciences, Okayama University, Okayama, Japan, [4]Monell Chemical Senses Center, Philadelphia, PA, USA.

Corresponding author:

Atsuko Yamashita, Graduate School of Medicine, Dentistry and Pharmaceutical Sciences, Okayama University, 1-1-1, Tsushima-naka, Kita-ku, Okayama 600-8530, Japan. Fax: +81-86-251-7974. E-mail: a_yama@okayama-u.ac.jp.

Abstract

Salt taste sensation is multifaceted: NaCl at low or high concentrations is preferably or aversively perceived through distinct pathways. Cl^- is thought to participate in taste sensation through an unknown mechanism. Here we describe Cl^- ion binding and the response of taste receptor type 1 (T1r), a receptor family composing sweet/umami receptors. The T1r2a/T1r3 heterodimer from the medaka fish, currently the sole T1r amenable to structural analyses, exhibited a specific Cl^- binding in the vicinity of the amino-acid-binding site in the ligand-binding domain (LBD) of T1r3, which is likely conserved across species, including human T1r3. The Cl^- binding induced a conformational change in T1r2a/T1r3LBD at sub- to low-mM concentrations similar to canonical taste substances. Furthermore, oral Cl^- application to mice increased impulse frequencies of taste nerves connected to T1r-expressing taste cells and promoted their behavioral preferences attenuated by a T1r-specific blocker or T1r3 knock-out. These results suggest that the Cl^- evokes taste sensations by binding to T1r, thereby serving as another preferred salt taste pathway at a low concentration.

36 **Introduction**

37 The taste sensation is initiated by specific interactions between chemicals in food and taste
38 receptors in taste buds in the oral cavity. In vertebrates, the chemicals are grouped into five
39 basic modalities: sweet, umami, bitter, salty, and sour. This sensation occurs through taste
40 receptor recognition specific to a group of chemicals representing each taste modality (Taruno
41 *et al*, 2021). Regarding the salty taste, the preferable taste, ~100 mM concentration of table salt,
42 is evoked by specific interaction between the epithelial sodium channel (ENaC) and sodium ion
43 (Chandrashekar *et al*, 2010) (Fig 1). Notably, salt sensation exhibits multifaced properties
44 (Roper, 2015), thereby suggesting the existence of an adequate concentration range for salt
45 intake to maintain the homeostasis of body fluid concentration. For example, high
46 concentrations of salt over levels perceived as a preferred taste, such as ~500 mM, stimulate
47 bitter and sour taste cells and are perceived as an aversive taste (Oka *et al*, 2013). Conversely,
48 low salt concentrations under the "preferable" concentration, such as several mM to a hundred
49 mM concentrations, are perceived as sweet by human panels (Bartoshuk *et al*, 1964; Bartoshuk
50 *et al*, 1978; Cardello, 1979). However, its mechanism has never been extensively pursued.

51

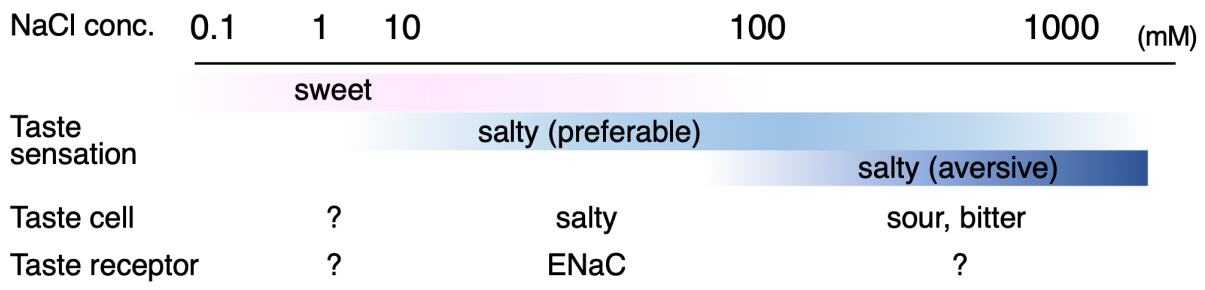

52

53

54 **Figure 1. Salt taste sensation.** Approximate concentration ranges of salt taste perceptions in
55 humans (Bartoshuk *et al.*, 1978) and qualities of taste sensation with known cells and receptors
56 responsible for their sensing are summarized.

57

58 The various impacts of the salt taste sensation indicate multiple salt detection pathways in taste
59 buds (Roper, 2015). Moreover, another component of table salt, the chloride ion, participates
60 in taste sensation because of the existence of the "anion effect": the salty taste is most strongly
61 perceived when the counter anion is a chloride ion (Ye *et al*, 1991). Several reports suggested
62 a certain cellular/molecular machinery underlying anion-sensitive Na^+-detection or Cl^--
63 detection, which is independent of ENaC (Lewandowski *et al*, 2016; Roebber *et al*, 2019).
64 Indeed, a recent study indicated that transmembrane channel-like 4 (TMC4) expressed in taste
65 buds involves high-concentration Cl^--sensation (Kasahara *et al*, 2021). Nevertheless, no
66 candidate molecule capable of sensing low or preferable concentrations of Cl^- has been
67 elucidated. Therefore, the complete understanding of salt taste sensation, including the
68 mechanism of chloride ion detection, remains unclear.

69 Unlike salt taste sensation, those for nutrients as sugars, amino acids, and nucleotides
70 are understood as sweet and umami sensations through specific receptor proteins (Li *et al*, 2002;
71 Nelson *et al*, 2002; Nelson *et al*, 2001). Sweet and umami receptors are composed of taste
72 receptor type 1 (T1r) proteins in the class C G protein-coupled receptor family. In humans, the
73 T1r1/T1r3 heterodimer serves as the umami taste receptor and responds to amino acids as L-
74 glutamate and aspartate, and nucleotides. In contrast, the T1r2/T1r3 heterodimer is the sweet
75 taste receptor and responds to sugars. We previously elucidated the crystallographic structure
76 of the medaka fish T1r2a/T1r3 extracellular ligand-binding domain (LBD) (Nuemket *et al*,
77 2017), which is currently the sole reported structure of T1rs. In the structure, the amino acid-
78 binding was observed in the middle of the LBD of T1r2a and T1r3 subunits, which was
79 consistent with the fact that T1r2a/T1r3 is an amino-acid receptor (Oike *et al*, 2007).
80 Furthermore, chloride ion binding was found in the vicinity of the amino-acid binding site in
81 T1r3 (Fig 2A). So far, the physiological significance of Cl^--binding for T1rs functions remains
82 unexplored. Nevertheless, chloride ions regulate other receptors in class C G protein-coupled

83 receptors (GPCRs), such as metabotropic glutamate receptors (mGluRs) and calcium-sensing
84 receptors (CaSRs), and act as positive modulators for agonist binding (Eriksen & Thomsen,
85 1995; Kuang & Hampson, 2006; Liu *et al*, 2020; Tora *et al*, 2018; Tora *et al*, 2015). The
86 potential effect of Cl^--binding on T1r receptor function is of significant interest under these
87 conditions.

88 Here, we investigated the Cl^- actions on T1rs using structural, biophysical, and
89 physiological analyses. The Cl^- binding to the LBD was investigated using the medaka fish
90 T1r2a/T1r3LBD, which is amenable to structural and biophysical analyses. Since the Cl^--
91 binding site in T1r3 was conserved across various species, taste nerve recordings from mice
92 were used to investigate the physiological significance of Cl^-. The results suggest that Cl^-
93 induces the moderate response via T1rs, thereby implying that T1rs are involved in Cl^-
94 sensation in taste buds.

95

96 **Results**

97 **Cl^--binding site in T1r3**

98 In the previously reported structure of T1r2a/T1r3LBD crystallized in the presence of NaCl,
99 bound Cl^- was identified based on electron density and binding distances (Nuemket *et al.*, 2017).
100 To verify the Cl^--binding, Cl^- in the T1r2a/T1r3LBD crystal was substituted with Br^-, a halogen
101 ion amenable for specific detection by anomalous scattering using a synchrotron light source
102 (Table S1). The diffraction data from the crystal resulted in an anomalous difference Fourier
103 peak at 14.1 σ at the site in the vicinity of the amino-acid binding site in T1r3, where Cl^- was
104 originally bound (Fig 2B, S1A). For further confirmation, the anomalous data of the original
105 crystal containing Cl^- was collected at 2.7 Å, where the anomalous peak for Cl and several
106 other elements such as Ca or S can be detected (Table S1). The resultant anomalous difference
107 Fourier map showed a peak at the bound Cl^- position, while all the other peaks were observed

108 at the S atoms in the protein (Fig 2C, S1B). These results verify that the site is able to bind

109 halogen ions, likely accommodating Cl^- under physiological conditions.

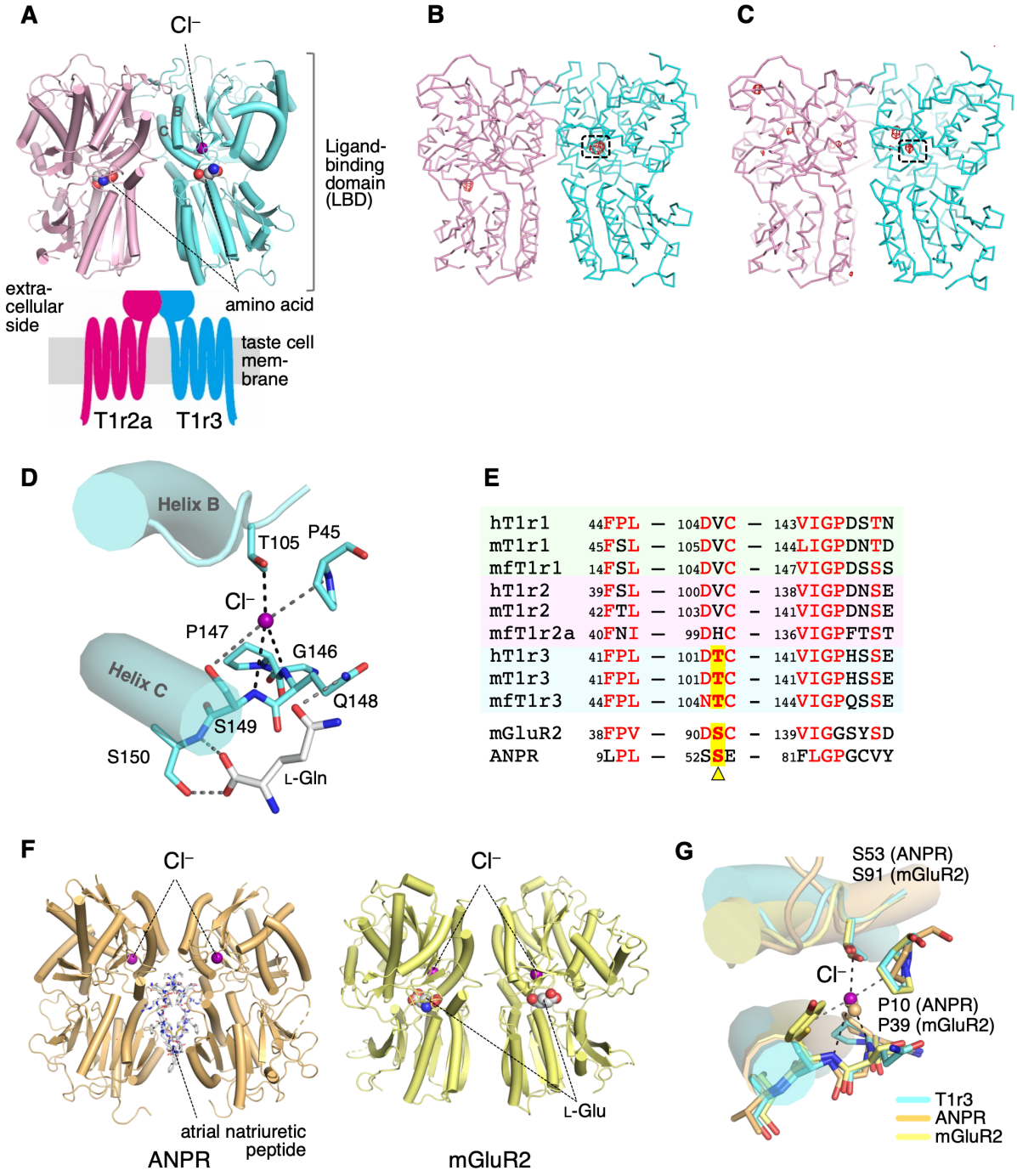

110

111 **Figure 2. Cl^--binding sites in the medaka fish taste receptor T1r2a/T1r3LBD.** (A)

112 Schematic drawing of the overall architecture of T1r2a/T1r3. The crystal structure (PDB ID:

113 5X2M) (Nuemket *et al.*, 2017) is shown at the LBD region, and helices B and C in T1r3 are

114 labeled. (B) Anomalous difference Fourier map (4.5 σ, red) of the Br^--substituted

115 T1r2a/T1r3LBD crystal. (C) Anomalous difference Fourier map (4.5 σ, red) of the Cl^--bound
116 T1r2a/T1r3LBD crystal derived from the diffraction data collected at the wavelength of 2.7 Å.
117 In panels B and C, the site originally identified the Cl^--binding was framed. (D) A close-up
118 view of the Cl^--binding site in T1r3LBD in the Cl^--bound T1r2a/T1r3LBD (PDB ID: 5X2M).
119 (E) Amino-acid sequence alignment of T1r proteins and the related receptors at the Cl^--binding
120 site. The "h," "m," and "mf" prefixes to T1rs indicate human, mouse, and medaka fish,
121 respectively. The position corresponding to Thr105 in T1r3 from medaka fish is highlighted.
122 (F) The structures of ANPR (PDB ID: 1T34, left) (Ogawa *et al*, 2004) and mGluR2 (PDB ID:
123 5CNI, right) (Monn *et al*, 2015a) bound with Cl^-. (G) Superposition of the Cl^--binding site in
124 T1r3, ANPR, and mGluR2.
125
126 Cl^- was coordinated at the binding site by the side-chain hydroxyl group of Thr105
127 and the main-chain amide groups of Gln148 and Ser149 (Fig 2D). These main-chain
128 coordinating residues are followed by Ser150, a critical residue for binding amino-acid ligands
129 (Nuemket *et al.*, 2017). Furthermore, the loop regions where Thr105 and the Gln148-Ser150
130 locate are followed by helices B and C, respectively. These helices are essential structural units
131 at the heterodimer interface (Nuemket *et al.*, 2017) (Fig 2A). They are known to reorient upon
132 agonist binding, resulting in conformation rearrangement of the subunits in the dimer, likely
133 inducing receptor activation in class C GPCRs (Koehl *et al*, 2019; Kunishima *et al*, 2000). In
134 addition, the side-chain hydroxyl group of Ser149, which serves as a cap for the positive helix
135 dipole of helix C, simultaneously functions as a distal ligand for Cl^- coordination. Therefore,
136 the Cl^- binding at this site is important for organizing the structure of the amino-acid binding
137 site and the heterodimer interface.
138 The Cl^--binding site observed in the crystal structure is most likely conserved among
139 T1r3s in various organisms, such as humans (Fig 2E). Thr105, the residue that provides the

140 side-chain-coordinating ligand for Cl^--binding, is strictly conserved as either serine or threonine
141 among T1r3s. Additionally, the amino-acid sequence motifs surrounding the main-chain-
142 coordinating ligands, $FP^{45}L$ and $VIGP\zeta^{148}\zeta^{149}$, where "ζ" is a hydrophilic amino acid, are well
143 conserved to present the main-chain amide groups to coordinate Cl^- with an appropriate
144 geometry. Notably, the site structurally corresponds to the Cl^--binding site in the hormone-
145 binding domain of the atrial natriuretic peptide receptor (ANPR) (Fig 2F, G), in which Cl^-
146 positively regulates the peptide hormone binding (Misono, 2000). Although ANPR is not a
147 member of class C GPCR, the hormone-binding domain in ANPR shares a similar structural
148 fold with LBD of T1rs and other class C GPCRs, and bacterial periplasmic-binding proteins
149 (Kunishima *et al.*, 2000; van den Akker *et al*, 2000). Accordingly, the conservation of the
150 structure and the sequence motif at the Cl^--binding site at ANPR is also observed on mGluRs
151 (Ogawa *et al*, 2010). Indeed, Cl^- binding at the site corresponding to that in T1r3 was observed
152 in several mGluR and CaSR structures (Monn *et al*, 2015b; Zhang *et al*, 2016) (Fig 2F, G) and
153 was identified as a potential site responsible for regulating agonist binding (Liu *et al.*, 2020;
154 Tora *et al.*, 2015). These results strongly imply the possibility that Cl^- has some actions on T1r
155 receptor functions.

156 In contrast, conservation at the Thr105 position was not observed among T1r1 and
157 T1r2 (Fig 2E). Evidently, no significant anomalous peak derived from Br^-- or Cl^--binding was
158 observed in the crystal structure at the corresponding site in T1r2a (Fig 2B, C). His100 in T1r2a,
159 which corresponds to Thr105 in T1r3, adopted a significantly different side-chain conformation
160 from that of Thr105 in T1r3 (Fig S1C). Therefore, T1r1 and T1r2's ability to bind Cl^- is unlikely.

161 In addition to the Cl^--binding site discussed above, the Br^--substituted crystal
162 exhibited an anomalous peak at 8.5 σ in T1r2a, at a position close to the Lys265 side-chain ε-
163 amino group (Fig 2B, S1D). Nevertheless, Cl^--binding was not observed in the original Cl^--
164 contained crystal. This is further confirmed by the absence of an anomalous peak at this position

165 in the data collected at 2.7 Å (Fig 2C, S1E). Therefore, the site might have the ability to bind
166 anions such as Br^- or larger; but be not specific to Cl^-. In human T1r1, the residue corresponding
167 to Lys265 (Arg277) was suggested as a critical residue for activities of inosine monophosphate,
168 an umami enhancer (Zhang *et al*, 2008).
169
170 **Cl^--binding properties in T1r2a/T1r3LBD**
171 To investigate the Cl^- actions on T1r functions, we first examined the properties of the Cl^--
172 binding to medaka T1r2a/T1r3LBD using various biophysical techniques. For this purpose, the
173 purified T1r2a/T1r3LBD was subjected to differential scanning fluorimetry (DSF), which we
174 previously used for the amino acid-binding analysis (Yoshida *et al*, 2019). In order to prepare
175 a Cl^--free condition, Cl^- in the sample was substituted with gluconate, as it is unlikely
176 accommodated in the Cl^--site due to its much larger size. We confirmed that gluconate does not
177 serve as a ligand for T1r2a/T1r3LBD (Fig S2A).
178 The addition of Cl^- to the Cl^--free T1r2a/T1r3LBD sample resulted in thermal
179 stabilization of the protein (Fig 3A), which is indicative of Cl^- binding to the protein. The
180 apparent K_d value for Cl^- estimated by the melting temperatures (T_m) at various Cl^-
181 concentrations was ~110 μM (Fig 3B, Table 1). The Cl^--dependent thermal stabilization was
182 confirmed by the fluorescence-detection size-exclusion chromatography-based thermostability
183 (FSEC-TS) assay (Hattori *et al*, 2012) (Fig 3C, Table 1). However, the Cl^--dependent
184 stabilization was not observed on T1r2a/T1r3 with the Cl^--site mutation, T105A in T1r3. In the
185 case of this mutant, the T_m values for both in the presence and absence of Cl^- was similar to the
186 values obtained for the wild-type protein in the absence of Cl^- (Fig 3C, S2B, Table 1). These
187 results indicate that the Cl^- effect attributed to the identical site where the Cl^--binding was
188 observed in the crystal structure of T1r3.
189

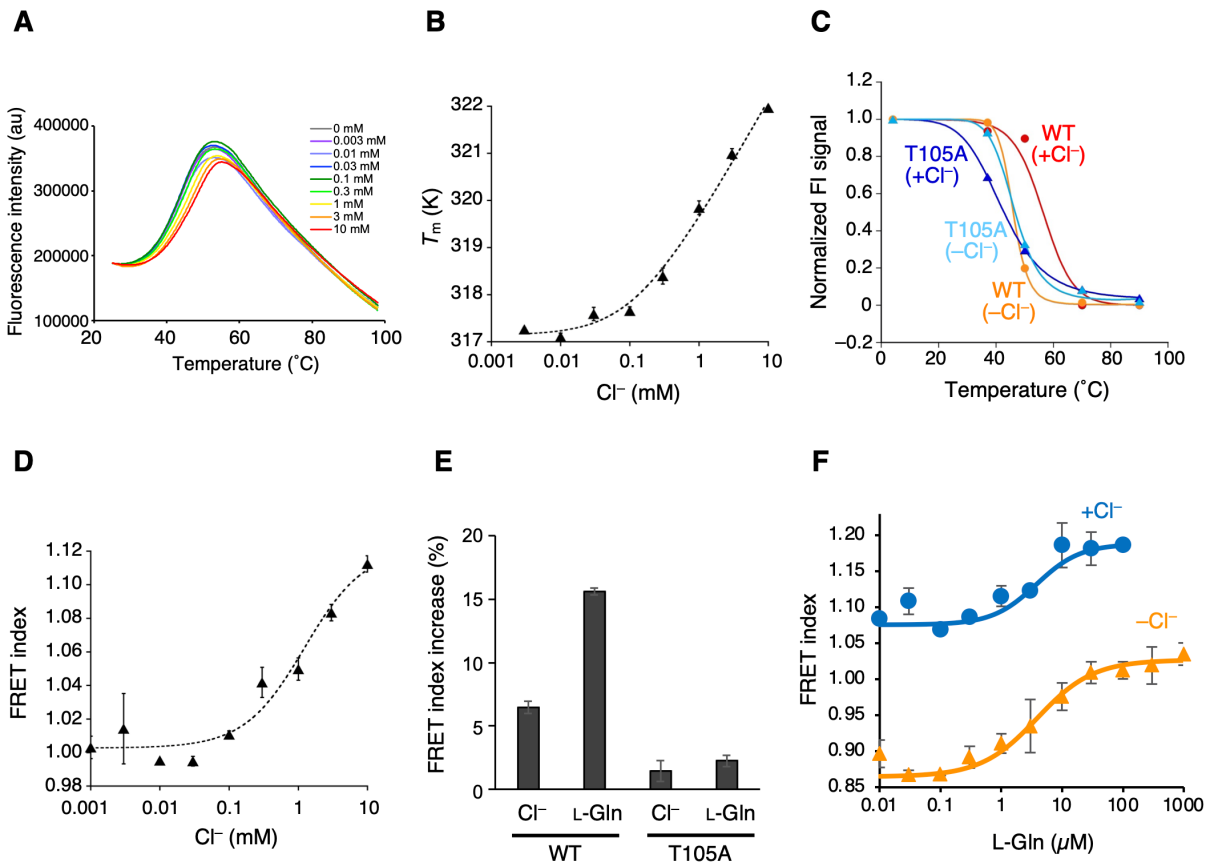

Figure 3. The Cl⁻-binding properties of T1r2a/T1r3LBD. (A) Representative thermal melt curves of T1r2a/T1r3LBD in the presence of 0.003 –10 mM concentrations of Cl^- measured using DSF. (B) Dose-dependent T_m changes of T1r2a/T1r3LBD by addition of Cl^-. (n = 4) (C) Thermal melting curves of WT and the T1r3-T105A mutant of T1r2a/T1r3LBD in the presence and absence of Cl^-, analyzed by FSEC-TS. (n = 1) (D) Dose-dependent FRET signal changes of the T1r2aLBD-Cerulean and T1r3LBD-Venus heterodimer by addition of Cl^-. (n = 3) (E) FRET index increases by adding 10-mM Cl^- or 1-mM L-glutamine to the WT or T1r3-T105A mutant T1r2aLBD-Cerulean/T1r3LBD-Venus heterodimer relative to that in the absence of any ligand in the absence of Cl^-. (n = 3) (F) Dose-dependent FRET signal changes of the T1r2aLBD-Cerulean and T1r3LBD-Venus heterodimer induced by the addition of L-glutamine in the presence and absence of Cl^-. (n = 3) The experiments were performed two (panels A, B, D, and E), three (C and WT), four (F and +Cl^- condition), or one (C and mutant; F and –Cl^- condition) time(s), and the results from one representative experiment are shown with numbers

204 of technical replicates. Data points represent mean and s.e.m.

205

206 **Table 1.** Properties of the Cl^--binding to T1r2a/T1r3LBD.

Cl^--binding, DSF (n = 4)		
$K_{d\text{-app}}$ (mM)	0.111 ± 0.046	
Protein thermal stability, DSF (n = 6)		
condition	$+Cl^-$	$-Cl^-$
Melting temperature (˚C)	55.2 ± 0.03	46.6 ± 0.06
Protein thermal stability, FSEC-TS		
wild type T1r2a/T1r3LBD (n = 3)		
condition	$+Cl^-$	$-Cl^-$
Melting temperature (˚C)	56.4 ± 5.1	46.0 ± 0.3
mutant T1r2a/T1r3-T105ALBD		
condition	$+Cl^-$	$-Cl^-$
Melting temperature (˚C)	42.7 ± 0.1	46.7 ± 0.7
Cl^-- binding, FRET (n = 3)		
FRET index minimum	1.00 ± 0.005	
FRET index change	0.119 ± 0.014	
EC_{50} (mM)*	1.23 ± 0.53	
L-glutamine binding, FRET (n = 3)		
condition	$+Cl^-$	$-Cl^-$
FRET index minimum	1.08 ± 0.01	0.86 ± 0.01
FRET index change	0.11	0.17
EC_{50} (μM)	3.78 ± 1.29	3.87 ± 1.76
Hill coefficient	1.20 ± 0.88	0.94 ± 0.29
L-glutamine binding, ITC		
condition	$+Cl^-$	$-Cl^-$
N (sites)	0.389 ± 0.028	0.303 ± 0.023
K_a (M^{-1})	$(2.85 \pm 0.65) \times 10^5$	$(2.12 \pm 0.46) \times 10^5$
[converted to K_d (μM)]	[3.51]	[4.72]
ΔH (kcal/mol)	−12.3 ± 1.2	–12.9 ± 1.3
ΔS (cal/mol/deg)	–16.3	−18.8

207 *Hill coefficient was fixed to 1 for fitting.

208 Next, we examined the consequence of the Cl^--binding to T1r2a/T1r3LBD via
209 Förster resonance energy transfer (FRET) using the fluorescent protein-fused sample. Class C
210 GPCRs commonly exhibit agonist-induced conformational changes in LBD, such as the dimer
211 rearrangement, which is essential for receptor activation and signaling (Ellaithy *et al*, 2020;
212 Koehl *et al.*, 2019; Kunishima *et al.*, 2000; Lin *et al*, 2021). Consistent with this, we previously
213 reported that T1r2a/T1r3LBD shows conformational change concomitant with the binding of
214 amino acids, which can be detected as increased FRET intensity (Nango *et al*, 2016). Notably,
215 adding Cl^- to the fluorescent protein-fused T1r2a/T1r3LBD also increased FRET intensities,
216 similar to amino acids (Fig 3D). The EC_{50} for Cl^--induced FRET signal change was determined
217 as ~1 mM (Table 1). Note that both DSF and FRET estimations have some degree of error: the
218 former produced slightly lower values than the latter, particularly in the case of weak affinities
219 in the mM concentration range (Yoshida *et al.*, 2019). As such, although the EC_{50} value
220 determined by FRET was slightly higher than the apparent K_d value of Cl^- determined by DSF,
221 the two are most likely relevant. Considering that the Cl^--binding site is located adjacent to the
222 dimer interface, which exhibits reorientation upon agonist binding (Fig 2D), the results suggest
223 that the Cl^-binding to T1r2a/T1r3LBD induces a conformational rearrangement of
224 T1r2a/T1r3LBD similar to its agonist amino acid. Nevertheless, the extent of the FRET change
225 induced by Cl^- was smaller than the changes induced by amino acids, such as ~1/2 of the latter
226 (Fig 3E). Therefore, the results suggest that the extent of the conformational change induced by
227 Cl^- is smaller than the change induced by amino acids. The extent of Cl^--dependent FRET index
228 change was reduced on T1r2a/T1r3 with the Cl^--site mutation, T105A in T1r3 (Fig 3E).
229 Considering that the amino-acid-dependent change in the mutant was also significantly reduced
230 (Fig 3E), the T105A mutation on T1r3 might result in losing the ability of the conformational
231 change induced by Cl^-- and amino-acid bindings, although the possibility of deactivation of the
232 protein during preparation due to its low stability cannot be excluded.

233 In addition to the Cl^--binding effect, the Cl^- effect on amino-acid binding to
234 T1r2a/T1r3LBD was investigated by FRET and isothermal calorimetry (ITC). The K_d values
235 for L-glutamine binding determined by ITC, as well as the EC_{50} values and the other parameters
236 for L-glutamine-induced conformational change determined by FRET, did not differ in the
237 presence and absence of Cl^- (Fig 3F, S2C, 2D, and Table 1). These results indicated that the Cl^-
238 binding had no significant effect on the binding of L-glutamine, a representative taste substance,
239 at least for T1r2a/T1r3LBD from medaka fish.
240
241 **Taste response to Cl^- through T1rs in mouse**
242 Biophysical studies on T1r2a/T1r3LBD from medaka fish suggested that Cl^-binding to
243 T1r3LBD induces a conformational change similar to that of an agonist without affecting
244 agonist binding. As described above, the Cl^--binding site is likely conserved among T1r3 in
245 various species, such as those in mammals. Therefore, we analyzed single fiber responses from
246 mouse chorda tympani nerve to investigate the physiological effect of Cl^- on taste sensation.
247 While conventional cell-based receptor assay systems are affected by changes in extracellular
248 ionic components, the application of various solutions to the taste pore side of the taste buds
249 projected to taste nerve systems, are transduced exclusively as "taste" signals, without inducing
250 the other cellular responses derived from the ionic component changes in the surrounding
251 environment.
252 We first identified nerve fibers that connect to T1r-expressing taste cells in wild-type
253 (WT) mice, i.e., that receive taste information from cells likely possessing sweet (T1r2/T1r3)
254 and umami (T1r1/T1r3) receptors (Yasumatsu *et al*, 2012). The identification was evidenced by
255 responses to T1r agonists, such as sugars and amino acids, which were inhibited by gurmarin
256 (Gur), a T1r-specific blocker (Daly *et al*, 2013; Margolskee *et al*, 2007; Ninomiya & Imoto,
257 1995; Ninomiya *et al*, 1999). Then, we examined the responses to Cl^- in these fibers.

258 Remarkably, the fibers also exhibited responses induced by Cl^-, which was applied as a form
259 of NMDG-Cl devoid of the known salty taste stimulant, sodium ion (Fig 4A). Cl^--induced
260 impulse frequencies from the nerves increased in a concentration-dependent manner (Fig 4B).
261 The responses to NMDG-Cl, NaCl, and KCl at the same concentrations did not differ
262 significantly (repeated measures analysis of variance [ANOVA], $P > 0.05$), whereas responses
263 to NMDG-gluconate were significantly smaller than those to NMDG-Cl (repeated measures
264 ANOVA: $F_{(1, 43)} = 31.33$, $P < 0.001$) and did not induce explicit responses up to 10 mM. These
265 results confirmed that the observed responses were attributed to Cl^-. All responses to Cl^-,
266 regardless of the type of counter cations, were significantly decreased by lingual treatment with
267 Gur (Fig 4B, repeated measures ANOVA: $F_{(1, 42)} = 56.65$, $P < 0.001$ for NMDG-Cl; $F_{(1, 50)} =$
268 24.78, $P < 0.001$ for NaCl; and $F_{(1, 45)} = 35.72$, $P < 0.001$ for KCl). Furthermore, responses to
269 Cl^- in T1r3-KO mice were significantly lower than those in WT mice (repeated measures
270 ANOVA: $F_{(1, 43)} = 25.36$, $P < 0.001$; Fig 4C). The results indicate that the observed Cl^--
271 dependent responses were mediated by T1r. Notably, the Cl^--concentration range that induced
272 nerve responses was lower (≤ ~10 mM) than that for Na^+-detection by ENaC when applied as
273 the NaCl form (≥ ~30 mM) (Chandrashekar *et al.*, 2010) but is consistent with those for Cl^--
274 binding and Cl^--induced conformational change observed on T1r2a/T1r3LBD (Table 1). These
275 results suggest that a low Cl^- concentration is sensorily detected via T1r in taste buds. Although
276 the responses induced by known taste substances for T1rs, such as sugars and amino acids,
277 range from tens to hundreds of impulse frequencies per 10 s (Yasumatsu *et al.*, 2012); the
278 maximum response level induced by Cl^- was low, ~10 per 10 s (Fig 4B). According to our
279 observations, Cl^- likely produces a "light" taste sensation compared with other known taste
280 substances.
281
282

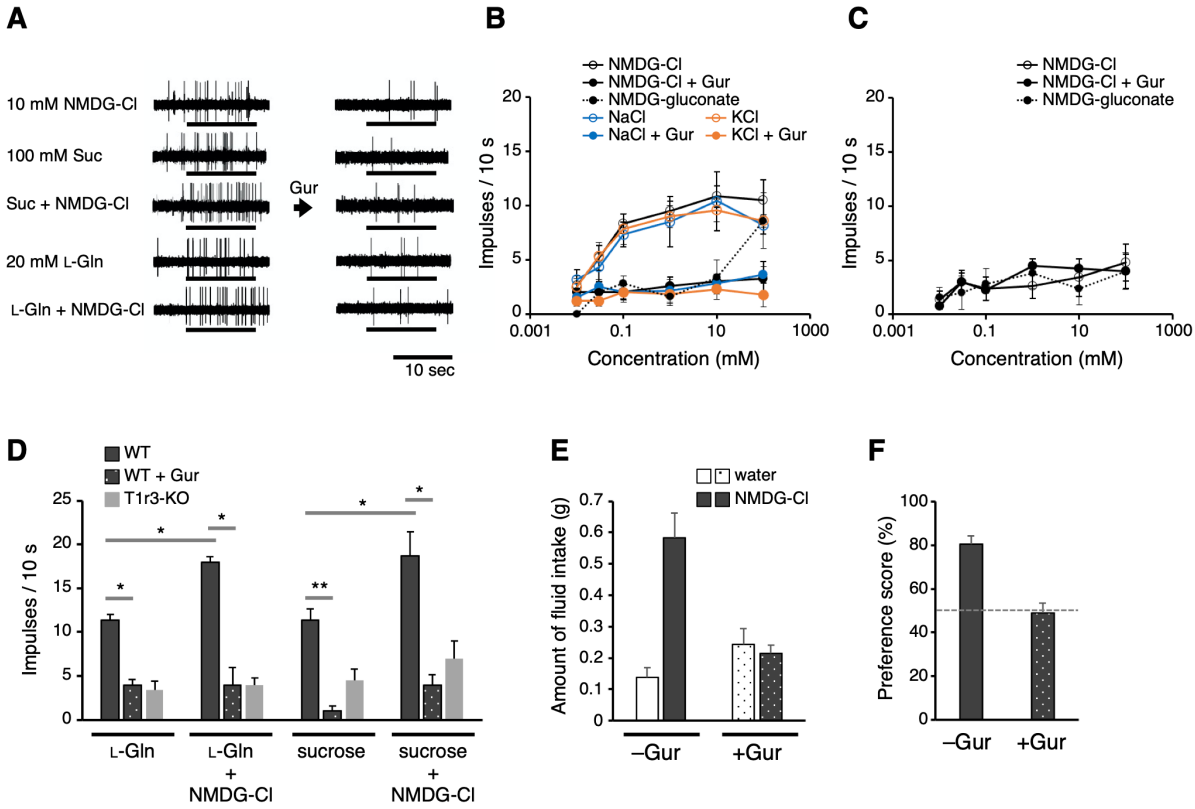

Figure 4. Electrophysiological and behavioral analyses of the T1r-mediated Cl⁻ responses in mouse. (A–D) Results of single fiber recordings from the mouse chorda tympani nerve. (A) Representative recordings of single fibers that connect to T1r-expressing taste cells. The stimuli were 10-mM NMDG-Cl, 100-mM sucrose, 100-mM sucrose + 10-mM NMDG-Cl, 20-mM L-glutamine, or 20-mM L-glutamine + 10-mM NMDG-Cl. Lines indicate the application of stimuli to the tongue. All the responses were suppressed by lingual treatment with a T1r blocker, Gur (right). (B) Impulse frequencies in response to the concentration series of NMDG-Cl, NaCl, or KCl before and after Gur treatment in WT mice. Responses to NMDG-gluconate are also shown. The mean number of net impulses per 10 s (mean response) ± s.e.m. in Gur-sensitive fibers (n = 5–6 from six mice). (C) Impulse frequencies in response to the concentration series of NMDG-Cl before and after Gur treatment were measured in T1r3-KO mice (n = 4–5 from three mice). Responses to NMDG-gluconate are also shown. (D) Impulse frequencies to 20-mM L-glutamine or 100-mM sucrose in the absence or presence of 10-mM NMDG-Cl before and after Gur treatment. Responses to 20-mM L-glutamine or 100-mM sucrose by T1r3-KO

298 mouse are also shown. Values are mean ± s.e.m. (n = 3–5 from three mice each). *, **: paired
299 t-test; $P < 0.05$ (*) and < 0.01 (**). (E) Amount of fluid intake for water and 10-mM NMDG-
300 Cl in the two-bottle preference tests. Values are mean ± s.e.m. (n = nine mice) (F) NMDG-Cl
301 intake shown in (E) normalized to water intake (preference score) in the two-bottle preference
302 tests. A score > 50% indicates that the taste solution was preferred over water.
303
304 Next, to examine the physiological interaction between a canonical taste substance
305 for mouse T1r and Cl^-, we recorded responses to 20-mM L-glutamine or 100-mM sucrose from
306 T1r1/T1r3- and T1r2/T1r3-expressing cells, respectively, with or without NMDG-Cl from the
307 same T1r-connecting single fibers (Fig 4A). The concentrations for the taste substances were
308 set to induce responses greater than the baseline but less than maximum. As shown in Figure
309 4D, the response to L-glutamine or sucrose increased significantly by adding 10-mM NMDG-
310 Cl (paired t-test, $t2 = 7.56$, $p = 0.017$ for L-glutamine and $t2 = 5.05$, $p = 0.037$ for sucrose). We
311 confirmed that these responses had been suppressed by a lingual treatment of Gur in the
312 presence ($t2 = 6.73$, $p = 0.021$ for L-glutamine and $t2 = 8.80$, $p = 0.013$ for sucrose) or absence
313 ($t2 = 8.32$, $p = 0.014$ for L-glutamine and $t2 = 11.72$, $p = 0.007$ for sucrose) of NMDG-Cl to a
314 similar extent. Moreover, the responses to the mixtures did not differ significantly from the
315 summation of the responses to each solution ($t2 = 2.34$, $p = 0.145$ for L-glutamine and $t2 = 2.31$,
316 $p = 0.147$ for sucrose). The results suggest that the simultaneous binding of Cl^- and a canonical
317 taste substance, such as amino acids and sugars, to T1r do not cause synergistic responses.
318 Finally, we addressed whether T1r-mediated Cl^- responses observed in the taste
319 nerves involve taste perception. Thus far, most reported behavioral assays for examining the
320 gustatory detection of NaCl were performed with concentrations above ~30 mM, which can
321 induce ENaC-mediated responses. Nevertheless, a few reports have shown that NaCl solution
322 induced higher consumption relative to water even below 10-mM concentration (Dyr *et al*,

323 2014; Stewart *et al*, 1994), which is below the range inducing ENaC-mediated responses
324 (Chandrashekar *et al.*, 2010) but within what we observed in the Cl^--induced taste nerve
325 responses via T1r. For verification, we performed a mouse two-bottle choice test using NMDG-
326 Cl solution and analyzed the preference relative to water. The mouse preferred water containing
327 10-mM NMDG-Cl, which was abolished by the application of Gur (Fig 4E, F). These results
328 suggest that Cl^- is preferably perceived through taste signal transduction mediated by T1r.
329

330 **Discussion**

331 In this study, Cl^- is found to specifically interact with the LBD in T1r3, a common component
332 of sweet and umami taste receptors, and induces a conformational change in the receptor's LBD
333 region. The Cl^- binding to T1r in taste cells is likely further transmitted to the sweet taste
334 nervous system, resulting in a light yet preferable taste sensation. Since T1rs are conserved
335 across vertebrates and the Cl^--binding site is likely conserved among T1r3 in various organisms,
336 T1r-mediated Cl^- responses might be common in many animals, such as humans. Evidently,
337 the concentration range for the Cl^--induced conformational change of medaka T1r2a/T1r3LBD
338 and increase in murine sweet nerve impulses observed in this study (i.e., ≤ ~10 mM) agrees
339 with the NaCl concentration perceived as "sweet" by humans (Bartoshuk *et al.*, 1964;
340 Bartoshuk *et al.*, 1978; Cardello, 1979) (Fig 1). Additionally, the sweet sensation induced by
341 NaCl was reportedly suppressed by topical application of *Gymnema sylvestre* (Bartoshuk *et al.*,
342 1978), containing Gymnemic acids, which are specific inhibitors of human sweet taste receptor
343 T1r2/T1r3 (Sanematsu *et al*, 2014). Overall, these results agree with the involvement of T1rs
344 in the Cl^--taste detection. These findings agree with an earlier hypothesis by Bartoshuk and
345 colleagues that dilute NaCl contains a sweet stimulus that interacts with the same receptor
346 molecules as sucrose (Bartoshuk *et al.*, 1978). The reported "sweet" sensation by low NaCl
347 concentration faded out at the concentrations detected as "salty" (Bartoshuk *et al.*, 1964;

348 Bartoshuk *et al.*, 1978; Cardello, 1979), thereby agreeing with the fact that we might be unaware
349 that table salt is sweet at such concentrations. The phenomenon could be explained by "mixture
350 suppression" (Bartoshuk, 1975; Keast & Breslin, 2002; Stevens, 1996), such that a light sweet
351 sensation is masked by an intense salty sensation in a higher concentration range of NaCl.

352 The Cl^- perception at low salt concentrations found in this study is achieved via the
353 T1rs-mediating taste system, which transduces information as a preferred taste by nature. Since
354 Cl^- is also a component of table salt, this system might serve as another pathway for preferred
355 salt perception promoting intake along with the pathway for Na^+ perception as a preferred taste
356 via taste cells that express the Na^+ receptor ENaC and a purinergic neurotransmission channel
357 CALHM1/3 (Nomura *et al*, 2020). In contrast, the T1r-mediated Cl^--sensing observed in this
358 study shows several different properties from those of cells or the molecules reportedly
359 exhibiting anion-sensitive Na^+ detection or Cl^- detection in taste buds thus far. Specifically, the
360 anion-sensitive Na^+-responding taste cells reported by Lewandowski *et al.* are type 3 cells,
361 which include sour- but not sweet-responding cells (Lewandowski *et al.*, 2016). The Cl^--
362 detection pathway reported by Roebber *et al.* was observed in type 2 cells, which include both
363 sweet- and bitter-responding cells, but was inhibited by a blocker of phospholipase C, which
364 mediates sweet- and bitter-signaling downstream of T1r and bitter receptors (Roebber *et al.*,
365 2019). The Cl^--responses mediated by TMC4 were observed in the glossopharyngeal nerve but
366 not in the chorda tympani nerve wherein T1r-mediated responses were observed (Kasahara *et*
367 *al.*, 2021). Notably, responses by these reported pathways were tested by much higher
368 concentrations of NaCl, typically in the several hundred mM range (Kasahara *et al.*, 2021;
369 Lewandowski *et al.*, 2016; Roebber *et al.*, 2019), than those used in this study. These results
370 imply that there may be multiple distinct concentration-dependent pathways for Cl^- detection
371 in taste buds. Given that high NaCl concentration is transduced as an aversive taste through
372 bitter and sour taste cells (Oka *et al.*, 2013), the relevance between the reported high Cl^--

373 responsive pathways and high NaCl responses by bitter and sour cells is of interest, as pointed
374 out by the previous studies, and will require further investigation.
375 Salt taste sensation and natriuresis are critical physiological processes that regulate
376 sodium intake and excretion to maintain body fluid homeostasis. Intriguingly, both processes
377 were found to use the counter anion Cl^- to regulate the molecular functions of the receptors,
378 T1rs and ANPRs, which share a similar extracellular protein architecture with a conserved Cl^-
379 -binding site. In the case of ANPR, mGluRs, and CaSR, positive allosteric modulations by Cl^-
380 for agonist binding have been observed, with some variations in the extent of the enhancement
381 (Eriksen & Thomsen, 1995; Kuang & Hampson, 2006; Liu *et al.*, 2020; Tora *et al.*, 2018; Tora
382 *et al.*, 2015). Whether the Cl^- actions on T1rs of other subtypes or from other organisms have
383 some variance is yet to be examined.
384
385 **Materials and methods**
386 **Crystallography**
387 All protein samples used for structural and functional analyses were prepared using Drosophila
388 S2 cells (Invitrogen) or high-expression clones for each protein sample established from S2
389 cells in previous studies (Nuemket *et al.*, 2017; Yamashita *et al*, 2017). No authentication or
390 test for mycoplasma contamination was performed.
391 The L-glutamine-bound T1r2a/T1r3LBD crystals, in complex with a crystallization
392 chaperone Fab16A, were prepared in the presence of NaCl as described (Nuemket *et al.*, 2017).
393 For the preparation of the Br^--substituted crystals, the obtained crystals were soaked in a mother
394 liquor consisting of 100 mM MES-Tris, pH 6.0, 50 mM NaBr, 17% PEG1500, 5% PEG400, 5
395 mM L-glutamine, 2 mM $CaCl_2$, cryoprotected by gradually increasing the concentration of
396 glycerol to 10%, incubated for 2 hours, and flash-frozen.
397 The X-ray diffraction data were collected at the SPring-8 beamline BL41XU using a

398 PILATUS6M detector (DECTRIS) at wavelength 0.9194 Å or at the Photon Factory beamline
399 BL-1A using an EIGER X4M detector (DECTRIS) at wavelength 2.7 Å. The data were
400 processed with XDS (Kabsch, 2010) (Table S1). The phases for anomalous difference Fourier
401 map calculation were obtained by molecular replacement methods with the program PHASER
402 (McCoy *et al*, 2007), using the structures of a single unit of the mfT1r2a-3LBD-Fab16A
403 complex (PDB ID: 5X2M; ligands and water models were removed) (Nuemket *et al.*, 2017) as
404 the search model (the R/R_{free} of the model for the Br^--data collected at 0.9194 Å: 0.248/0.350;
405 the Cl^--data collected at 2.7 Å: 0.233/0.339).
406
407 **Differential scanning fluorimetry (DSF)**
408 Differential scanning fluorimetry was performed as previously described (Yoshida *et al.*, 2019).
409 The purified mfT1R2a/3LBD heterodimer protein was prepared (Nango *et al.*, 2016) and
410 dialyzed with buffer A (20 mM HEPES-NaOH, 300 mM sodium gluconate, pH 7.5) to remove
411 Cl^-. 1 μg of the dialyzed protein sample was mixed with Protein Thermal Shift Dye (Applied
412 Biosystems) and 0.003 – 10 mM NaCl in 20 μL of buffer A. The mixture solutions were then
413 loaded to a MicroAmpR Fast Optical 48-Well Reaction Plate (Applied Biosystems).
414 Fluorescent intensities were measured by the StepOne Real-Time PCR System (Applied
415 Biosystems) while the temperature raised from 25 °C to 99 °C with a velocity of 0.022 °C/sec.
416 For detection, the reporter and quencher were set as "ROX" and "none," respectively. The
417 apparent melting transition temperature (T_m) was determined using the maximum of the
418 derivatives of the melt curve (dFluorescence/dT) by Protein Thermal Shift Software version 1.3
419 (Applied Biosystems). The apparent dissociation constant ($K_{d\text{-app}}$) for Cl^- derived from the T_m
420 values at different NaCl concentrations was estimated using a thermodynamic model proposed
421 by Schellman (Schellman, 1975) as described (Yoshida *et al.*, 2019). The sample sizes for the
422 analyses by DSF, as well as Förster resonance energy transfer and isothermal titration

423 calorimetry described below, were set to obtain reliable values based on the experiences in the
424 previous studies (Nango *et al.*, 2016; Nuemket *et al.*, 2017; Yoshida *et al.*, 2019).
425
426 **Förster resonance energy transfer (FRET)**
427 FRET analysis was performed as described previously (Nango *et al.*, 2016; Nuemket *et al.*,
428 2017). The WT T1r2aLBD-Cerulean and T1r3LBD-Venus fusion heterodimer proteins were
429 prepared as described (Nuemket *et al.*, 2017). For the mutant protein preparation, a T1r3-T105A
430 mutation was introduced into the vector pAc-mfT1r3aL-Ve (Nango *et al.*, 2016) using
431 polymerase chain reaction. The mutant expression vector was co-introduced with pAc-
432 mfT1r2aL-Ce (Nango *et al.*, 2016) to Drosophila S2 cells using Polyethyleneimine (PEI)
433 "MAX" (Polysciences) as previously described (Bleckmann *et al*, 2019) with a ratio of 0.5-μg
434 pAc-mfT1r2aL-Ce, 0.5-μg pAc- mfT1r3aL-Ve-T105A, and 10-μg PEI to ~1 × 10^6 cells.
435 Protein expression and purification were conducted similarly as for the WT protein.
436 For the Cl^--titration, the purified protein samples were dialyzed against buffer A in
437 the presence of 1-mM L-alanine. Afterward, the samples were diluted with buffer A to reduce
438 the remaining L-alanine concentration below 1 μM (< ~1/100 of EC_{50} (Nango *et al.*, 2016;
439 Nuemket *et al.*, 2017)), and then incubated in the presence of 0.001–10-mM NaCl or 1-mM L-
440 glutamine in buffer A at 4°C overnight. For L-glutamine titration in the presence or absence of
441 Cl^-, the protein solution was dialyzed with buffer B (20-mM HEPES-Tris, 300-mM NaCl, pH
442 7.5) or buffer C (20-mM HEPES-Tris, 300-mM sodium gluconate, pH 7.5) in the presence of
443 1-mM L-alanine to prepare the conditions with or without Cl^-, respectively. Then, the samples
444 were diluted with buffer B or C to reduce the remaining L-alanine concentration below 1-μM
445 and then incubated in the presence of 0.01–1000-μM L-glutamine at 4°C overnight.
446 Fluorescence spectra were recorded at 298 K with a FluoroMax4 spectrofluorometer (Horiba).
447 The sample was excited at 433 nm, and FRET was detected via the emission at 526 nm. The

448 emission at 475 nm was also recorded for the FRET index calculation. The FRET index
449 (intensity at 526 nm/intensity at 475 nm) was plotted against the Cl^- or L-glutamine
450 concentration, and the titration curves were fitted to the Hill equation using KaleidaGraph
451 (Synergy Software) or ORIGIN (OriginLab).
452
453 **Isothermal titration calorimetry**
454 In order to prepare the conditions with or without Cl^-, the purified mfT1R2a/3LBD heterodimer
455 protein was dialyzed with buffers B or C, respectively. The dialyzed protein solution (~50 μM)
456 was then loaded into the sample cell in iTC200 (GE Healthcare) after the removal of insoluble
457 materials by centrifugation (10,000×*g*, 15 min, 277 K). The titration was performed by injecting
458 2 μL of 400 μM L-glutamine at intervals of 120 s at 298 K. The thermograms and the binding
459 isotherms were analyzed with Origin software, assuming one set of binding sites for fitting.
460
461 **Fluorescence-detection size-exclusion chromatography-based thermostability assay**
462 **(FSEC-TS)**
463 A T1r3-T105A mutation was introduced in the vector pAc_mfT1r3L (Yamashita *et al.*, 2017)
464 by PCR. The mutant expression vector was co-introduced with pAc_mft1r2aL (Yamashita *et*
465 *al.*, 2017) to Drosophila S2 cells to establish a stable high-expression clone cell as previously
466 described (Yamashita *et al.*, 2017). The wild-type T1r2a/T1r3LBD and mutant T1r2a/T1r3-
467 105A-LBD proteins were expressed and purified as previously described (Nango *et al.*, 2016)
468 with several modifications as listed below. After the protein binding to ANTI-FLAG M2 affinity
469 gel, the resin was washed with either buffer D (20 mM HEPES-NaOH, 0.3 M NaCl, 2 mM
470 $CaCl_2$, 5 mM L-Gln, pH 7.5) or buffer E (20 mM HEPES-NaOH, 0.3 M Na gluconate, 2 mM
471 Ca gluconate, 5 mM L-Gln, pH 7.5). Then, the protein was eluted with 100 μg/mL FLAG
472 peptide in buffer D or E.

473 The protein solutions (50 μg/mL) in buffer D or E were incubated at 4 °C, 37 °C,
474 50 °C, 70 °C, or 90 °C at 2 hours. Subsequently, the samples were loaded on an SEC-5 column,
475 500 Å, 4.6 × 300 mm (Agilent) connected to a Prominence HPLC system (Shimadzu), using
476 buffer D or E as a running buffer at a flow rate of 0.3 ml min^{-1}. The elution profiles were
477 detected with an RF-20A fluorometer (Shimadzu), using excitation and emission wavelengths
478 of 280 and 340 nm for the detection of intrinsic tryptophan fluorescence.

479 The residual ratio after incubation at each temperature was estimated using the
480 fluorescence intensity at the elution peak, which corresponded to the T1rLBD dimer, *i.e.,* the
481 peak height at ~11.6 min. The values were normalized to the intensity of the sample incubated
482 at 4 °C as 1. In order to estimate the apparent melting temperature ($T_{m\text{-app}}$) of the sample, the
483 values of residual ratio at each temperature were fitted to the Gibbs-Helmholtz equation
484 transformed as shown below (assuming that the sample protein is under equilibrium between a
485 folding and unfolding state under each condition):

486 $$Residual\ ratio = 1 - \frac{1}{1 + exp\left[-\frac{\Delta H\left(1 + \frac{T}{T_{m-app}}\right) - \Delta C_P\left\{\left(T_{m-app} - \mathrm{T}\right) + Tln\left(\frac{T}{T_{m-app}}\right)\right\}}{RT}\right]}$$

487 where ΔH and ΔC_p are the enthalpy and heat capacity change of unfolding, respectively; T is
488 the temperature of the sample incubation; R is the gas constant. The fittings were performed
489 with KaleidaGraph (Synergy Software), with ΔH, ΔC_p, and $T_{m\text{-app}}$ are set as valuables.

490

491 **Single fiber recording from mouse chorda tympani (CT) nerve**

492 All animal experiments were conducted following the National Institutes of Health Guide for
493 the Care and Use of Laboratory Animals and approved by the committee for Laboratory Animal
494 Care and Use and the local ethics committee at Tokyo Dental College and Okayama University
495 Japan. The subjects were six adult male C57BL/6JCrj mice (Charles River Japan, Tokyo, Japan)
496 and four T1r3GFP-KO mice, which were obtained by mating T1r3-GFP (Damak *et al*, 2008)

497 and T1r3-KO (Damak *et al*, 2003) mice. Mice were maintained on a 12/12-h light/dark cycle
498 and fed standard rodent chow and 8–20 weeks of age ranging in weight from 20 g to 30 g.
499 The mice were anesthetized with an injection of sodium pentobarbital (40–50 mg/kg
500 ip) and maintained at a surgical level of anaesthesia, with additional injections (8–10 mg/kg ip
501 every hour). Under anaesthesia, each mouse was fixed in the supine position with a head holder,
502 and the trachea cannulated. The right CT nerve was dissected, free from surrounding tissues,
503 after the removal of the pterygoid muscle and cut at the point of its entry to the tympanic bulla.
504 A single or a few nerve fibers were teased apart with a pair of needles and lifted onto an Ag-
505 AgCl electrode, and an indifferent electrode was placed in nearby tissue. Their neural activities
506 were amplified (K-1; Iyodenshikagaku, Nagoya, Japan) and recorded on a computer using a
507 PowerLab system (PowerLab/sp4; AD Instruments, Bella Vista, NSW, Australia). For taste
508 stimulation of fungiform papillae, the anterior half of the tongue was enclosed in a flow
509 chamber. Taste solutions or rinses (distilled water) (~24 °C) were delivered to the tongue by
510 gravity flow at the same flow rate (~0.1 mL s^{-1}). For data analysis, we used the net average
511 frequency for 10 sec after the stimulus onset, which was obtained by subtracting the
512 spontaneous frequency for the 10 sec duration before stimulation from after stimulation. In the
513 initial survey to identify a nerve fiber connecting to T1r-expressing cells, test stimuli such as
514 100 mM NaCl, 10 mM HCl, 500 mM sucrose, 100 mM monopotassium glutamate, 20 mM
515 quinine HCl were separately applied. If the fiber responded to sucrose, we applied 10 μM–100
516 mM NMDG-Cl, NaCl, KCl, or either of 20 mM L-glutamine or 100 mM sucrose with or without
517 10 mM NMDG-Cl to the tongue. The criteria for the occurrence of response were the following:
518 the number of spikes was larger than the mean + two standard deviations of the spontaneous
519 discharge for three 10-s periods before stimulation, and at least three spikes were evoked by
520 taste stimulation (Yasumatsu *et al.*, 2012). In the case of T1r3GFP-KO mice, as the mice
521 showed a significant response to 0.5-M sucrose, we could identify sweet-responsive fibers

522 (impulse frequency of 13.4 ± 1.31) (Yasumatsu *et al.*, 2012). The reagents used were purchased
523 from Wako Pure Chemical Industries (Osaka, Japan; others). To block responses via T1r (Daly
524 *et al.*, 2013; Margolskee *et al.*, 2007; Ninomiya & Imoto, 1995; Ninomiya *et al.*, 1999), each
525 tongue was treated with 30-μg ml^{-1} (~7 μM) gurmarin (Gur) dissolved in 5-mM phosphate
526 buffer (pH 6.8) for 10 min, similarly as described by Ninomiya & Imoto (Ninomiya & Imoto,
527 1995). To assure the detection of responses from T1r-expressing cells, recordings from Gur-
528 insensitive sweet-responsive fibers were defined as those retaining impulse frequencies to 0.5-
529 M sucrose more than 60% after the Gur treatment (Ninomiya *et al.*, 1999) were excluded from
530 the data. The number of Gur-sensitive and Gur-insensitive fibers were six and three,
531 respectively, among 0.5-M sucrose responding fibers. The sucrose application was repeated 3–
532 6 times during the recordings. Additionally, the recovery of the suppressed responses was
533 confirmed using 15-mM β-cyclodextrin, which could remove the effect of Gur from the tongue
534 (Ninomiya *et al.*, 1999). All Gur-sensitive fibers recovered up to 60%–150% of responses
535 before Gur. At the end of the experiment, animals were killed by administering an overdose of
536 the anaesthetic. Repeated measures ANOVA and Student's paired *t*-test were used to statistically
537 evaluate the effects of chemicals or gene deletion. The sample size was calculated according to
538 power analysis, thereby resulting in three per group due to the effect size (d) of 6–9.3 to detect
539 the effects of blocking or deleting T1r3.
540
541 **Two-bottle preference tests**
542 All training and testing sessions occurred during the light phase of the light/dark cycle. On the
543 first day of training, the WT mice (adult male C57BL/6JCrj) were water deprived for 23 h and
544 then placed in a test box with two bottles: one filled with water and the other empty. The amount
545 of fluid intake was measured after a 5-min presentation. After 4 days of training, mice were
546 used for test sessions if they drank water evenly on either side (nine mice). In the test sessions,

547 they were provided with two bottles, one containing 10-mM NMDG-Cl and the other
548 containing water, with or without Gur, for 5 min. The amount of liquid consumed was measured
549 by weighing the bottles, and a preference score of NMDG-Cl was calculated using the following
550 equation:

551 $$Preference\ score(\%) = \frac{V_{Cl}}{V_{Cl} + V_w} \times 100$$

552 where V_{cl} and V_w are the amount of NMDG-Cl intake and water intake, respectively.

553

554 **Acknowledgments**

555 We thank Drs. Kazuya Hasegawa, Nobuhiro Mizuno, Naohiro Matsugaki for help with X-ray
556 data collection; Junya Nitta and Hikaru Ishida for help with protein preparation; Ryusuke
557 Yoshida for help with the single fiber recording; Yuko Kusakabe for attempt at cell-based
558 receptor assay in the early stage of the study; Haruo Ogawa for sharing knowledge about ANPR;
559 Yuzo Ninomiya for valuable discussions. We also thank the reviewers of BioPhysics Colab for
560 their helpful comments and Enago (www.enago.jp) for the English language review. The
561 synchrotron radiation experiments at the BL41XU, SPring-8 were performed with approvals of
562 the Japan Synchrotron Radiation Research Institute (JASRI) (Proposal No. 2016B2534). The
563 synchrotron radiation experiment at the BL-1A, Photon Factory was supported by the Platform
564 for Drug Discovery, Informatics, and Structural Life Science (Proposal No. 1264). This work
565 was financially supported by JSPS KAKENHI Grant Numbers JP17H03644, JP18H04621,
566 JP20H03195, JP20H04778, JP21H05524 (to A.Y.) and JP20H03855 (to K.Y.), Mishima Kaiun
567 Memorial Foundation, and the Salt Science Research Foundation (Proposal No. 2039) (to A.Y.).

568

569 **Competing interests**

570 The authors declare that they have no conflict of interest.

571

572 **References**

573 Bartoshuk LM (1975) Taste mixtures: is mixture suppression related to compression? *Physiol*
574 *Behav* 14: 643-649
575 Bartoshuk LM, McBurney DH, Pfaffmann C (1964) Taste of Sodium Chloride Solutions after
576 Adaptation to Sodium Chloride: Implications for the "Water Taste". *Science* 143: 967-968
577 Bartoshuk LM, Murphy C, Cleveland CT (1978) Sweet taste of dilute NaCl: psychophysical
578 evidence for a sweet stimulus. *Physiol Behav* 21: 609-613
579 Bleckmann M, Schurig M, Endres M, Samuels A, Gebauer D, Konisch N, van den Heuvel J
580 (2019) Identifying parameters to improve the reproducibility of transient gene expression in
581 High Five cells. *PLoS One* 14: e0217878
582 Cardello AV (1979) Taste quality changes as a function of salt concentration in single human
583 taste papillae. *Chem Senses* 4: 1-13
584 Chandrashekar J, Kuhn C, Oka Y, Yarmolinsky DA, Hummler E, Ryba NJ, Zuker CS (2010)
585 The cells and peripheral representation of sodium taste in mice. *Nature* 464: 297-301
586 Daly K, Al-Rammahi M, Moran A, Marcello M, Ninomiya Y, Shirazi-Beechey SP (2013)
587 Sensing of amino acids by the gut-expressed taste receptor T1R1-T1R3 stimulates CCK
588 secretion. *Am J Physiol Gastrointest Liver Physiol* 304: G271-282
589 Damak S, Mosinger B, Margolskee RF (2008) Transsynaptic transport of wheat germ agglutinin
590 expressed in a subset of type II taste cells of transgenic mice. *BMC Neurosci* 9: 96
591 Damak S, Rong M, Yasumatsu K, Kokrashvili Z, Varadarajan V, Zou S, Jiang P, Ninomiya Y,
592 Margolskee RF (2003) Detection of sweet and umami taste in the absence of taste receptor T1r3.
593 *Science* 301: 850-853
594 Dyr W, Wyszogrodzka E, Mierzejewski P, Bienkowski P (2014) Drinking of flavored solutions
595 by high preferring (WHP) and low preferring (WLP) alcohol-drinking rats. *Pharmacol Rep* 66:
596 28-33
597 Ellaithy A, Gonzalez-Maeso J, Logothetis DA, Levitz J (2020) Structural and Biophysical
598 Mechanisms of Class C G Protein-Coupled Receptor Function. *Trends Biochem Sci* 45: 1049-
599 1064
600 Eriksen L, Thomsen C (1995) [3H]-L-2-amino-4-phosphonobutyrate labels a metabotropic
601 glutamate receptor, mGluR4a. *Br J Pharmacol* 116: 3279-3287
602 Hattori M, Hibbs RE, Gouaux E (2012) A fluorescence-detection size-exclusion
603 chromatography-based thermostability assay for membrane protein precrystallization screening.
604 *Structure* 20: 1293-1299
605 Kabsch W (2010) Xds. *Acta Crystallogr D Biol Crystallogr* 66: 125-132
606 Kasahara Y, Narukawa M, Ishimaru Y, Kanda S, Umatani C, Takayama Y, Tominaga M, Oka Y,

607 Kondo K, Kondo T *et al* (2021) TMC4 is a novel chloride channel involved in high-
608 concentration salt taste sensation. *J Physiol Sci* 71: 23
609 Keast RS, Breslin PA (2002) An overview of binary taste–taste interactions. *Food Quality and*
610 *Preference* 14: 111-124
611 Koehl A, Hu H, Feng D, Sun B, Zhang Y, Robertson MJ, Chu M, Kobilka TS, Laeremans T,
612 Steyaert J *et al* (2019) Structural insights into the activation of metabotropic glutamate receptors.
613 *Nature* 566: 79-84
614 Kuang D, Hampson DR (2006) Ion dependence of ligand binding to metabotropic glutamate
615 receptors. *Biochem Biophys Res Commun* 345: 1-6
616 Kunishima N, Shimada Y, Tsuji Y, Sato T, Yamamoto M, Kumasaka T, Nakanishi S, Jingami H,
617 Morikawa K (2000) Structural basis of glutamate recognition by a dimeric metabotropic
618 glutamate receptor. *Nature* 407: 971-977
619 Lewandowski BC, Sukumaran SK, Margolskee RF, Bachmanov AA (2016) Amiloride-
620 Insensitive Salt Taste Is Mediated by Two Populations of Type III Taste Cells with Distinct
621 Transduction Mechanisms. *J Neurosci* 36: 1942-1953
622 Li X, Staszewski L, Xu H, Durick K, Zoller M, Adler E (2002) Human receptors for sweet and
623 umami taste. *Proc Natl Acad Sci U S A* 99: 4692-4696
624 Lin S, Han S, Cai X, Tan Q, Zhou K, Wang D, Wang X, Du J, Yi C, Chu X *et al* (2021) Structures
625 of Gi-bound metabotropic glutamate receptors mGlu2 and mGlu4. *Nature* 594: 583-588
626 Liu H, Yi P, Zhao W, Wu Y, Acher F, Pin JP, Liu J, Rondard P (2020) Illuminating the allosteric
627 modulation of the calcium-sensing receptor. *Proc Natl Acad Sci U S A* 117: 21711-21722
628 Margolskee RF, Dyer J, Kokrashvili Z, Salmon KS, Ilegems E, Daly K, Maillet EL, Ninomiya
629 Y, Mosinger B, Shirazi-Beechey SP (2007) T1R3 and gustducin in gut sense sugars to regulate
630 expression of Na+-glucose cotransporter 1. *Proc Natl Acad Sci U S A* 104: 15075-15080
631 McCoy AJ, Grosse-Kunstleve RW, Adams PD, Winn MD, Storoni LC, Read RJ (2007) Phaser
632 crystallographic software. *J Appl Crystallogr* 40: 658-674
633 Misono KS (2000) Atrial natriuretic factor binding to its receptor is dependent on chloride
634 concentration: A possible feedback-control mechanism in renal salt regulation. *Circ Res* 86:
635 1135-1139
636 Monn JA, Prieto L, Taboada L, Hao J, Reinhard MR, Henry SS, Beadle CD, Walton L, Man T,
637 Rudyk H *et al* (2015a) Synthesis and Pharmacological Characterization of C4-(Thiotriazolyl)-
638 substituted-2-aminobicyclo[3.1.0]hexane-2,6-dicarboxylates. Identification of
639 (1R,2S,4R,5R,6R)-2-Amino-4-(1H-1,2,4-triazol-3-ylsulfanyl)bicyclo[3.1.0]hexane-2, 6-
640 dicarboxylic Acid (LY2812223), a Highly Potent, Functionally Selective mGlu2 Receptor
641 Agonist. *J Med Chem* 58: 7526-7548

642 Monn JA, Prieto L, Taboada L, Pedregal C, Hao J, Reinhard MR, Henry SS, Goldsmith PJ,
643 Beadle CD, Walton L *et al* (2015b) Synthesis and pharmacological characterization of C4-
644 disubstituted analogs of 1S,2S,5R,6S-2-aminobicyclo[3.1.0]hexane-2,6-dicarboxylate:
645 identification of a potent, selective metabotropic glutamate receptor agonist and determination
646 of agonist-bound human mGlu2 and mGlu3 amino terminal domain structures. *J Med Chem*
647 58: 1776-1794
648 Nango E, Akiyama S, Maki-Yonekura S, Ashikawa Y, Kusakabe Y, Krayukhina E, Maruno T,
649 Uchiyama S, Nuemket N, Yonekura K *et al* (2016) Taste substance binding elicits
650 conformational change of taste receptor T1r heterodimer extracellular domains. *Sci Rep* 6:
651 25745
652 Nelson G, Chandrashekar J, Hoon MA, Feng L, Zhao G, Ryba NJ, Zuker CS (2002) An amino-
653 acid taste receptor. *Nature* 416: 199-202
654 Nelson G, Hoon MA, Chandrashekar J, Zhang Y, Ryba NJ, Zuker CS (2001) Mammalian sweet
655 taste receptors. *Cell* 106: 381-390
656 Ninomiya Y, Imoto T (1995) Gurmarin inhibition of sweet taste responses in mice. *Am J Physiol*
657 268: R1019-1025
658 Ninomiya Y, Imoto T, Sugimura T (1999) Sweet taste responses of mouse chorda tympani
659 neurons: existence of gurmarin-sensitive and -insensitive receptor components. *J Neurophysiol*
660 81: 3087-3091
661 Nomura K, Nakanishi M, Ishidate F, Iwata K, Taruno A (2020) All-Electrical Ca(2+)-
662 Independent Signal Transduction Mediates Attractive Sodium Taste in Taste Buds. *Neuron* 106:
663 816-829 e816
664 Nuemket N, Yasui N, Kusakabe Y, Nomura Y, Atsumi N, Akiyama S, Nango E, Kato Y, Kaneko
665 MK, Takagi J *et al* (2017) Structural basis for perception of diverse chemical substances by T1r
666 taste receptors. *Nat Commun* 8: 15530
667 Ogawa H, Qiu Y, Ogata CM, Misono KS (2004) Crystal structure of hormone-bound atrial
668 natriuretic peptide receptor extracellular domain: rotation mechanism for transmembrane signal
669 transduction. *J Biol Chem* 279: 28625-28631
670 Ogawa H, Qiu Y, Philo JS, Arakawa T, Ogata CM, Misono KS (2010) Reversibly bound
671 chloride in the atrial natriuretic peptide receptor hormone-binding domain: possible allosteric
672 regulation and a conserved structural motif for the chloride-binding site. *Protein Sci* 19: 544-
673 557
674 Oike H, Nagai T, Furuyama A, Okada S, Aihara Y, Ishimaru Y, Marui T, Matsumoto I, Misaka
675 T, Abe K (2007) Characterization of ligands for fish taste receptors. *J Neurosci* 27: 5584-5592
676 Oka Y, Butnaru M, von Buchholtz L, Ryba NJ, Zuker CS (2013) High salt recruits aversive

677 taste pathways. *Nature* 494: 472-475
678 Roebber JK, Roper SD, Chaudhari N (2019) The Role of the Anion in Salt (NaCl) Detection by
679 Mouse Taste Buds. *J Neurosci* 39: 6224-6232
680 Roper SD (2015) The taste of table salt. *Pflugers Arch* 467: 457-463
681 Sanematsu K, Kusakabe Y, Shigemura N, Hirokawa T, Nakamura S, Imoto T, Ninomiya Y
682 (2014) Molecular mechanisms for sweet-suppressing effect of gymnemic acids. *J Biol Chem*
683 289: 25711-25720
684 Schellman JA (1975) Macromolecular Binding. *Biopolymers* 14: 999-1018
685 Stevens JC (1996) Detection of tastes in mixture with other tastes: issues of masking and aging.
686 *Chem Senses* 21: 211-221
687 Stewart RB, Russell RN, Lumeng L, Li TK, Murphy JM (1994) Consumption of sweet, salty,
688 sour, and bitter solutions by selectively bred alcohol-preferring and alcohol-nonpreferring lines
689 of rats. *Alcohol Clin Exp Res* 18: 375-381
690 Taruno A, Nomura K, Kusakizako T, Ma Z, Nureki O, Foskett JK (2021) Taste transduction and
691 channel synapses in taste buds. *Pflugers Arch* 473: 3-13
692 Tora AS, Rovira X, Cao AM, Cabaye A, Olofsson L, Malhaire F, Scholler P, Baik H, Van
693 Eeckhaut A, Smolders I *et al* (2018) Chloride ions stabilize the glutamate-induced active state
694 of the metabotropic glutamate receptor 3. *Neuropharmacology* 140: 275-286
695 Tora AS, Rovira X, Dione I, Bertrand HO, Brabet I, De Koninck Y, Doyon N, Pin JP, Acher F,
696 Goudet C (2015) Allosteric modulation of metabotropic glutamate receptors by chloride ions.
697 *FASEB J* 29: 4174-4188
698 van den Akker F, Zhang X, Miyagi M, Huo X, Misono KS, Yee VC (2000) Structure of the
699 dimerized hormone-binding domain of a guanylyl-cyclase-coupled receptor. *Nature* 406: 101-
700 104
701 Yamashita A, Nango E, Ashikawa Y (2017) A large-scale expression strategy for multimeric
702 extracellular protein complexes using Drosophila S2 cells and its application to the recombinant
703 expression of heterodimeric ligand-binding domains of taste receptor. *Protein Sci* 26: 2291-
704 2301
705 Yasumatsu K, Ogiwara Y, Takai S, Yoshida R, Iwatsuki K, Torii K, Margolskee RF, Ninomiya
706 Y (2012) Umami taste in mice uses multiple receptors and transduction pathways. *J Physiol*
707 590: 1155-1170
708 Ye Q, Heck GL, DeSimone JA (1991) The anion paradox in sodium taste reception: resolution
709 by voltage-clamp studies. *Science* 254: 724-726
710 Yoshida T, Yasui N, Kusakabe Y, Ito C, Akamatsu M, Yamashita A (2019) Differential scanning
711 fluorimetric analysis of the amino-acid binding to taste receptor using a model receptor protein,

712 the ligand-binding domain of fish T1r2a/T1r3. *PLoS One* 14: e0218909
713 Zhang C, Zhang T, Zou J, Miller CL, Gorkhali R, Yang JY, Schilmiller A, Wang S, Huang K,
714 Brown EM *et al* (2016) Structural basis for regulation of human calcium-sensing receptor by
715 magnesium ions and an unexpected tryptophan derivative co-agonist. *Sci Adv* 2: e1600241
716 Zhang F, Klebansky B, Fine RM, Xu H, Pronin A, Liu H, Tachdjian C, Li X (2008) Molecular
717 mechanism for the umami taste synergism. *Proc Natl Acad Sci U S A* 105: 20930-20934
718